# Mass Residuals as a Criterion for Mesh Refinement in Continuous Galerkin Shallow Water Models

J. C. Dietrich[1]; R. L. Kolar, M.ASCE[2]; and K. M. Dresback[3]

**Abstract:** Mass balance error has been computed traditionally by using conventional fluxes derived from the conservation of mass equation, but recent literature supports a method based on fluxes that are consistent with the discretization of the governing equations. By comparing the mass residuals from these two methods to the truncation errors produced by the discretization of the governing equations, we show that the conventional fluxes produce mass residuals that are more descriptive of the overall behavior of the model, i.e., they are better correlated with truncation error. Then we demonstrate that these mass residuals can be used as a criterion for mesh refinement. In an example using a one-dimensional shallow water model, we demonstrate that, by moving nodes from regions with large mass residuals to regions with small mass residuals, a mesh can be developed that shows less truncation error than a mesh developed by using localized truncation error analysis. And, in an example using a two-dimensional shallow water model, we demonstrate that the computed solution can be improved in regions with large mass residuals through mesh refinement.

**DOI:** 10.1061/(ASCE)0733-9429(2008)134:5(520)

**CE Database subject headings:** Mesh generation; Numerical models; Hydrodynamics; Finite element method; Shallow water.

## Background

The use of norms for error diagnosis has a long and diverse history. Gresho and Lee (1981) argued that oscillatory solutions are "good" in that they provide motivation for reexamination of boundary conditions, geometry, meshing, and problem formulation. By examining the errors in a computed solution, it is possible to identify parts of the model that require improvement. Researchers have applied this idea in the areas of mesh generation and refinement. Some researchers refine meshes by examining the solution or its derivatives (Behrens 1998; Cascon et al. 2003; Marrocu and Ambrosi 1999; Wille 1998). These adaptive meshing techniques use a posteriori error estimators that are based on the computed response, and they have been applied successfully in shallow water applications. However, because these techniques are based on solution error, which often involves a discrete estimate of the gradient of the computed response, they can reintroduce truncation error.

Other researchers generate meshes based on a localized truncation error analysis (LTEA), which minimizes phasing and amplitude errors (Hagen et al. 2000, 2001). In the review of adaptive mesh strategies by Baker (1997), the author mentions earlier uses of truncation error as a meshing criterion (Berger and Jameson 1985; Berger and Oliger 1984; Lee and Tsuei 1993) but notes that "[s]urprisingly, this approach to error estimation does not appear to have gained much acceptance." One possible reason is that it is costly to develop these grids because they require a priori calculation of the truncation errors, which require knowledge of the "true" solution, typically obtained from a uniformly and highly refined mesh. And, like the adaptive strategies above, these strategies require a discrete estimate of derivatives, albeit on a finer mesh, so truncation error is minimized.

In this paper, we examine the use of mass residuals as a criterion for mesh refinement. Mass conservation must be a consideration for any shallow water model, but it is especially important for continuous Galerkin finite-element models, such as the advanced circulation (ADCIRC) family of models used in the numerical examples in this paper (Luettich and Westerink 1992; Luettich and Westerink, unpublished online user's manual, 2004). In particular, continuous Galerkin finite-element models can suffer from global or local mass error (Lynch 1985). Global mass balance errors can be eliminated through proper treatment of the boundary conditions (Lynch 1985; Kolar et al. 1996). However, local mass errors can persist in complex applications, such as regions with rapidly converging/diverging flow or wetting and drying (Kolar et al. 1994; Horritt 2002). In addition, local mass errors are acutely problematic when a shallow water model is coupled to a transport model. If water mass is not conserved, then the transport model will show artificial gains or losses in the mass of the transported species. Minimization of these local mass residuals would improve the behavior of the shallow water model in all of these applications. Furthermore, and in contrast to mesh refinement based on LTEA, mesh refinement based on mass residuals does not require knowledge of the forms of the truncation error terms and does not require a highly resolved background grid (Hagen et al. 2000, 2001). Thus, it has the potential to be performed in real time, to improve resolution in wetting and dry-

[1]Graduate Student, Dept. of Civil Engineering and Geological Sciences, Univ. of Notre Dame, 156 Fitzpatrick Hall, Notre Dame, IN 46556 (corresponding author). E-mail: dietrich.15@nd.edu

[2]Professor, School of Civil Engineering and Environmental Science, Univ. of Oklahoma, 202 W. Boyd St., Room 334, Norman, OK 73019. E-mail: kolar@ou.edu

[3]Research Associate, School of Civil Engineering and Environmental Science, Univ. of Oklahoma, 202 W. Boyd St., Room 334, Norman, OK 73019. E-mail: dresback@ou.edu

Note. Discussion open until October 1, 2008. Separate discussions must be submitted for individual papers. To extend the closing date by one month, a written request must be filed with the ASCE Managing Editor. The manuscript for this paper was submitted for review and possible publication on September 13, 2005; approved on September 14, 2007. This paper is part of the ***Journal of Hydraulic Engineering***, Vol. 134, No. 5, May 1, 2008. ©ASCE, ISSN 0733-9429/2008/5-520–532/ $25.00.

ing regions as a storm surge inundates and recedes, for example.

We examine this criterion in the framework of two research questions. First: Which mass residual is a better indicator of truncation errors? Second: Can this mass residual be used as a criterion for mesh refinement?

Recent literature disagrees about the best method to compute local mass residuals in models based on the continuous Galerkin finite-element method; specifically, there is disagreement about how best to compute flux. A conventional method of computing flux would begin with the conservation of mass equation and evaluate a boundary integral, which in one dimension gives the familiar $Q=HU$, where $Q$=flux; $H$=total water depth; and $U$=depth-averaged velocity (Kolar et al. 1994). However, in models based on the continuous Galerkin finite-element method, mass conservation is enforced globally. Thus, when the conventional fluxes are computed locally in those models, the fluxes may not necessarily conserve mass because they are not consistent with the finite-element discretization of the governing equations (Hughes et al. 2000; Berger and Howington 2002). Instead, it is possible to derive fluxes that are consistent with the discretization and that conserve mass locally. In this paper, we derive both the conventional flux and consistent fluxes for the one-dimensional ADCIRC model, and then we examine how well the respective residuals correlate with local truncation errors. If these mass residuals do indeed correlate with local truncation errors, then they might be used as a mesh refinement criterion.

In the sections that follow, we derive the fluxes and their respective error norms, examine their correlation with local truncation errors in two test cases, and demonstrate the development of a computational mesh based on the minimization of mass residuals, both in one and two dimensions. These analyses will be conducted with the ADCIRC family of models (Kolar and Westerink 2000), which have found use in a variety of applications, ranging from storm surge calculations to ecosystem studies (Westerink et al. 2008; Luettich et al. 1999). ADCIRC is based on the generalized wave continuity (GWC) equation and the continuous Galerkin finite-element method. The GWC equation was first developed by Lynch and Gray (1979) and Kinnmark (1984, 1985), and it employs a numerical parameter $G$ that weights the contributions of the wave equation and the primitive continuity equation to prevent spurious oscillations. However, ADCIRC's implementation of the GWC equation is not dissimilar from shallow water models based on the continuity equation; for example, if the numerical parameter $G$ is selected carefully, then the discretization of the GWC equation can be shown to be equivalent to the discretization of the continuity equation using the quasi-bubble scheme employed by Telemac (Mewis and Holtz 1993; Atkinson et al. 2004). Furthermore, the results herein can be applied to other shallow water models, such as Norton et al. (1973) or Lynch et al. (1996), which are based on the continuous Galerkin finite-element method. In any model that does not enforce mass conservation locally, the mass residuals might be useful as a criterion for mesh refinement.

## Methods

### Mass Residuals

The algorithm to evaluate mass conservation was presented by one of the writers in a previous work (Kolar et al. 1994); it is repeated here for completeness. The conservation of mass equation reduces to the depth-averaged continuity equation under shallow water assumptions, to get

$$\frac{\partial \zeta}{\partial t} + \nabla \cdot (H\mathbf{U}) = 0 \tag{1}$$

where $\zeta$=departure of the water surface elevation from the mean; $\nabla$=gradient operator in two dimensions; $H$=total water depth; and $\mathbf{U}$=depth-averaged velocity. Integrate Eq. (1) over space and time to obtain

$$\int_{t_0}^{t} \int_{\Omega} \left[ \frac{\partial \zeta}{\partial t} + \nabla \cdot (H\mathbf{U}) \right] d\Omega \, dt = 0 \tag{2}$$

where $\Omega$=entire domain (for a global check of mass conservation) or one element or a patch of elements (for a local check of mass conservation); $t$=time; and $t_0$=reference time, such as the beginning of the simulation. The first term in Eq. (2) is integrated over time and the divergence theorem is applied to the second term to obtain

$$\int_{\Omega} (\zeta_t - \zeta_0) d\Omega + \int_{t_0}^{t} \left[ \int_{\partial\Omega} H\mathbf{U} \cdot \mathbf{n} \, d(\partial\Omega) \right] dt = 0 \tag{3}$$

where the first term represents accumulation and the second term represents net flux. Now we approximate the dependent variables with their discrete counterparts. For the first term in Eq. (3), we approximate $\zeta$ with linear Lagrange basis functions and evaluate exactly the integral as

$$\int_{\Omega} (\zeta_t - \zeta_0) d\Omega = \sum_e [\overline{\zeta_t} - \overline{\zeta_{t_0}}]_e A_e \tag{4}$$

where $A_e$=area of element $e$; $\overline{\zeta}$=arithmetic average of the nodal values of $\zeta$ over the element; and the sum is over all elements in the domain of interest.

For the second term in Eq. (3), the boundary integral represents the net flux into the domain, where $\mathbf{n}$=unit outward normal vector. There is disagreement in the literature about the best method to compute this net flux. For now, we define

$$Q_{\text{net}} = \int_{\partial\Omega} H\mathbf{U} \cdot \mathbf{n} \, d(\partial\Omega) \tag{5}$$

and then we approximate the second term in Eq. (3) using the trapezoidal rule

$$\int_{t_0}^{t} \left[ \int_{\partial\Omega} H\mathbf{U} \cdot \mathbf{n} \, d(\partial\Omega) \right] dt = \int_{t_0}^{t} Q_{\text{net}} \, dt \approx \sum_k \frac{1}{2} [Q_{\text{net}}^{t+\Delta t} + Q_{\text{net}}^{t}] \Delta t \tag{6}$$

where $k$=time step index. Note that, in order to keep the derivation more general, the above relations were derived for a two-dimensional model; they can be simplified easily to their one-dimensional counterparts. In the ensuing derivation, the point of departure will be the one-dimensional equations in order to keep the mathematics tractable.

Thus, for a single one-dimensional element to conserve mass locally over one time step, it would have to satisfy exactly this equation

$$(\overline{\zeta_{t+\Delta t}} - \overline{\zeta_t}) \Delta x_e + \tfrac{1}{2} (Q_{\text{net}}^{t+\Delta t} + Q_{\text{net}}^{t}) \Delta t = 0 \tag{7}$$

where $\Delta x_e$=length of the element. If any residual error exists, then it would appear as a nonzero sum.

Debate in the literature centers around how to evaluate the net flux, $Q_{\text{net}}$, defined in Eq. (5). We examine two methods of computing fluxes. The first method evaluates the boundary integral in Eq. (5) using exact quadrature. Thus, in one dimension, the integral reduces to point evaluations of $H$ and $\mathbf{U}$ at the boundaries of the element

$$Q_{\text{net},V} \equiv \int_{\partial\Omega} H\mathbf{U}\cdot\mathbf{n}\,d(\partial\Omega) = -H_L U_L + H_R U_R \tag{8}$$

where the subscripts $L$ and $R$ denote left and right boundaries of a one-dimensional element, respectively; and the subscript $V$ indicates that these fluxes are denoted as conventional fluxes. Because it is based on the continuous Galerkin method and the GWC equation, the ADCIRC model does not enforce locally the mass conservation equation shown in Eq. (1). Our first error measure uses Eq. (7) and the conventional fluxes from Eq. (8) to obtain

$$\varepsilon_V = \left|(\overline{\zeta_{t+\Delta t}} - \overline{\zeta_t})\Delta x_e + \tfrac{1}{2}(Q^{t+\Delta t}_{\text{net},V} + Q^{t}_{\text{net},V})\Delta t\right| \tag{9}$$

where $\varepsilon_V$=mass balance residual. This residual is not normalized to the still water volume in the element or the departure from the still water volume in the element. We examine only the magnitudes of these residuals for ease of comparison with the local truncation errors, for reasons explained below.

The second method solves for fluxes in a manner that is consistent with the Galerkin finite-element formulation of the GWC equation. According to Hughes et al. (2000) and Berger and Howington (2002), fluxes computed in this manner are locally conservative. A comprehensive derivation of these fluxes for the one-dimensional ADCIRC model can be found in Dietrich et al. (unpublished internal report, 2006); we include the significant steps here. Begin with the one-dimensional form of the GWC equation

$$\frac{\partial^2\zeta}{\partial t^2} + G\frac{\partial\zeta}{\partial t} - HU\frac{\partial G}{\partial x} - \frac{\partial}{\partial x}\left[\frac{\partial}{\partial x}(HUU) + gH\frac{\partial\zeta}{\partial x} - E_l\frac{\partial^2}{\partial x^2}(HU) + \tau HU - GHU\right] = 0 \tag{10}$$

where $G$=numerical parameter introduced by Kinnmark (1985, 1986); $g$=gravitational constant; $E_l$=lateral eddy viscosity; and $\tau$=bottom friction parameter, here assumed to be a constant and to have units of $\text{sec}^{-1}$. Note that, for all of the test cases herein, the eddy viscosity has been assumed to be constant. For convenience, we replace the quantity in brackets with the dummy variable $A$, multiply by the linear Lagrange weight function associated with node $i$, and integrate over two elements containing node $i$ to obtain

$$\int_{x_{i-1}}^{x_i}\left(\frac{\partial^2\zeta}{\partial t^2} + G\frac{\partial\zeta}{\partial t} - HU\frac{\partial G}{\partial x} - \frac{\partial A}{\partial x}\right)\phi_i\,dx + \int_{x_i}^{x_{i+1}}\left(\frac{\partial^2\zeta}{\partial t^2} + G\frac{\partial\zeta}{\partial t} - HU\frac{\partial G}{\partial x} - \frac{\partial A}{\partial x}\right)\phi_i\,dx = 0 \tag{11}$$

Apply integration by parts to the last term in both integrals to obtain

$$\int_{x_{i-1}}^{x_i}\left[\left(\frac{\partial^2\zeta}{\partial t^2} + G\frac{\partial\zeta}{\partial t} - HU\frac{\partial G}{\partial x}\right)\phi_i + A\frac{d\phi_i}{dx}\right]dx - (A\phi_i)|_{x_i^-} + \int_{x_i}^{x_{i+1}}\left[\left(\frac{\partial^2\zeta}{\partial t^2} + G\frac{\partial\zeta}{\partial t} - HU\frac{\partial G}{\partial x}\right)\phi_i + A\frac{d\phi_i}{dx}\right]dx + (A\phi_i)|_{x_i^+} = 0 \tag{12}$$

where we have utilized $\phi_i(x_{i-1})=0$ and $\phi_i(x_{i+1})=0$. In the two boundary terms, the superscripts indicate contributions from the left (−) or right (+) of the node. By substituting the one-dimensional forms of the conservation equations for mass and momentum, we can simplify the dummy variable $A$ in those boundary terms to

$$\int_{x_{i-1}}^{x_i}\left[\left(\frac{\partial^2\zeta}{\partial t^2} + G\frac{\partial\zeta}{\partial t} - HU\frac{\partial G}{\partial x}\right)\phi_i + A\frac{d\phi_i}{dx}\right]dx + \left[\left(\frac{\partial Q}{\partial t} + GQ\right)\phi_i\right]\Bigg|_{x_i^-} + \int_{x_i}^{x_{i+1}}\left[\left(\frac{\partial^2\zeta}{\partial t^2} + G\frac{\partial\zeta}{\partial t} - HU\frac{\partial G}{\partial x}\right)\phi_i + A\frac{d\phi_i}{dx}\right]dx - \left[\left(\frac{\partial Q}{\partial t} + GQ\right)\phi_i\right]\Bigg|_{x_i^+} = 0 \tag{13}$$

where $Q$=flux through node $i$. In an example by Berger and Howington (2002) of the advective transport of a conservative tracer, only the flux $Q$ appears in the boundary terms, and thus they are able to solve for fluxes that are both locally conservative and continuous at the nodes. However, the GWC equation is a derivative form of the shallow water equations, which gives rise to the $\partial Q/\partial t + GQ$ term on the boundary. Thus, we are unable to enforce continuity of flux directly at each node; rather, we enforce continuity of the quantity $\partial Q/\partial t + GQ$. To do so, we require

$$\left(\frac{\partial Q}{\partial t} + GQ\right)\Bigg|_{x_i^-} = -\int_{x_{i-1}}^{x_i}\left(\frac{\partial^2\zeta}{\partial t^2}\phi_i + G\frac{\partial\zeta}{\partial t}\phi_i - HU\frac{\partial G}{\partial x}\phi_i + A\frac{d\phi_i}{dx}\right)dx \tag{14}$$

and

$$\left(\frac{\partial Q}{\partial t} + GQ\right)\Bigg|_{x_i^+} = \int_{x_i}^{x_{i+1}}\left(\frac{\partial^2\zeta}{\partial t^2}\phi_i + G\frac{\partial\zeta}{\partial t}\phi_i - HU\frac{\partial G}{\partial x}\phi_i + A\frac{d\phi_i}{dx}\right)dx \tag{15}$$

Eqs. (14) and (15) can be thought of as ordinary differential equations that can be solved for $Q$, in a manner similar to Massey and Blain (2006). It should be noted that the resulting discrete flux equations are quite complex, involving many terms, and thus it is not possible to attach the same physical interpretation that was done for the conventional fluxes shown in Eq. (8). However, in the limit as $G\to\infty$, the fluxes at the boundary can be recovered in terms of just $Q$.

Using these consistent fluxes, we can solve for the net flux in an element

$$Q_{\text{net},S} = -Q_L + Q_R = -Q_{x_i^+} + Q_{x_{i+1}^-} \tag{16}$$

where the flux $Q_{x_i^+}$ corresponds to the right side of node $i$, and the flux $Q_{x_{i+1}^-}$ corresponds to the left side of node $i+1$. (The flux is

continuous across node $i$ only if $Q_{x_i^+}=Q_{x_{i+1}^-}$). Then define a second error measure

$$\varepsilon_S = |(\overline{\zeta_{t+\Delta t}} - \overline{\zeta_t})\Delta x_e + \tfrac{1}{2}(Q^{t+\Delta t}_{\text{net},S} + Q^{t}_{\text{net},S})\Delta t| \quad (17)$$

where $\varepsilon_S$=mass balance residual when the net fluxes $Q_{\text{net},S}$ are evaluated using the consistent flux statement given in Eq. (16). (Note that we are using the subscript $V$ to denote conVentional and the subscript $S$ to denote conSistent.)

Note that the error norms defined in Eqs. (9) and (17) are dimensional. They could be normalized to the deviation from the still water volume of the element by dividing by $\overline{\zeta_{t+\Delta t}}\Delta x_e$, where $\overline{\zeta_{t+\Delta t}} \equiv (\zeta_{L,t+\Delta t}+\zeta_{R,t+\Delta t})/2$=average at time $t+\Delta t$ of the water surface elevation departures from the mean for the nodes on the left ($L$) and right ($R$) of a one-dimensional element, and $\Delta x_e$=length of that element. However, this normalization is counterproductive in the framework of this work, where the goal is to establish a mass residual that can be used as a criterion for mesh refinement. If the error norm is related inversely to the mesh spacing, i.e., if decreases in the mass residual in the numerator are offset by decreases in the mesh spacing in the denominator, then the error norm may not converge as the mesh is refined. In fact, in our experience, the normalized mass residuals have sometimes increased as the mesh is refined, which is not the case for the residuals as they are defined above. In short, normalization of the residuals masks the actual error in the domain and limits inter-mesh comparisons. For those reasons, we use the non-normalized residuals herein.

We stress the importance of the flux discontinuities at the nodes. This result is a significant departure from the results presented by Berger and Howington (2002), and it calls into question the utility of the consistent flux approach. Mass conservation is necessary in transport applications, but those applications require a continuous flux in order to conserve information from one element to the next. Without a continuous flux, the perfect elemental mass conservation given by the consistent fluxes is lost. In order to examine this behavior in the context of the GWC equation with respect to local truncation errors and mesh refinement, we define the discontinuity

$$\delta_S = |Q_{x_i^+} - Q_{x_i^-}| \quad (18)$$

which becomes our third error norm. In contrast to the mass balance residuals defined in Eqs. (9) and (17), the discontinuity defined in Eq. (18) is nodal based.

### Truncation Errors

ADCIRC is based on two equations: the GWC equation, which is a derivative form of the mass conservation equation; and the non-conservative form of the momentum equation (NCM). The GWC equation is shown in Eq. (10). The NCM equation in one dimension is

$$\frac{\partial U}{\partial t} + U\frac{\partial U}{\partial x} + \tau U + g\frac{\partial \zeta}{\partial x} - \frac{E_l}{H}\frac{\partial^2}{\partial x^2}(HU) = 0 \quad (19)$$

where the variables are defined previously. In the one-dimensional form of the ADCIRC model, the GWC and NCM equations are discretized using linear Lagrange basis functions and a Galerkin finite-element scheme in space, a Crank–Nicolson scheme on the linear terms in time, and an explicit formulation for the nonlinear terms in time. We utilize exact quadrature rules and an $L_2$ interpolation for the advective terms. Full details for the higher-dimensional forms of ADCIRC can be found in Luettich and Westerink (unpublished online user's manual, 2004).

Truncation error expressions for every term in the equations were developed by expanding in a Taylor series about a common interior node point. Use of a symbolic manipulator, such as Mathematica, allows us to carry out the analysis with confidence up to any order for the full nonlinear equations (which require products of Taylor series). These truncation error expressions can be found in Dresback and Kolar (unpublished internal report, 2004) or in Dresback (2005). A qualitative examination of these expressions shows that the GWC and NCM equations are first-order accurate in time, first-order accurate in space for variable node spacing, and second-order accurate in space for constant node spacing. The NCM equation becomes second-order accurate in time if the equation is linearized.

A quantitative examination of the truncation error expressions requires information from both fine and coarse grid solutions. For example, the first term in the GWC equation is the time derivative term, $\partial^2\zeta/\partial t^2$. In its truncation error expression, the leading order term is second order in time and is given by

$$\frac{1}{36}(\Delta x_j - \Delta x_{j-1})(\Delta t)^2 \frac{\partial^5 \zeta_{j,k}}{\partial x\, \partial t^4} \quad (20)$$

where $j$=spatial index; and $k$=temporal index. To approximate the derivatives that appear in the truncation error expressions, we use second-order central difference schemes on a fine grid (true) solution, which is obtained by refining the grid until the solution converges to the sixth decimal place. To evaluate the rest of the terms in the expressions, such as the nonderivative components in Eq. (20), we use information from a coarse grid solution, namely, a coarse grid spacing, time step, and parameter values. The truncation errors for all terms in the GWC and NCM equations are summed and compared against the mass residuals $\varepsilon_V$ and $\varepsilon_S$ and the flux discontinuity $\delta_S$, as computed from the coarse grid simulation. Note that we examine the magnitudes of these truncation errors, to prevent cancellation of errors due to opposite signs.

For the ensuing discussion, it is useful to think of the truncation error expression in Eq. (20) as containing a derivative part and a grid/parameter part. For all of the truncation error terms, the derivative part is independent of the coarse grid discretization and thus fixed (for a given domain and a given simulation). And it is evaluated by using a true solution, which in our case is a fine grid solution that remains the same for all coarse discretizations. Regardless of the coarse grid that is used to discretize this domain, these values from the derivative parts of the errors will persist. However, because the algorithm is consistent, the product of the grid/parameter and derivative parts goes to zero in the limit as the grid is refined.

On the other hand, the grid/parameter component of each truncation error term is dependent on the discretization and other user-selected parameters. A modeler can manipulate this component to alter algorithm behavior. In fact, some grids are designed to minimize the coarse component in regions where the fine component is large (and vice versa), so that the overall truncation error is uniform throughout the computational domain (Hagen et al. 2000, 2001).

## Analyses in One Dimension

We examine initially the relationships between our error norms and local truncation errors using a one-dimensional test based on

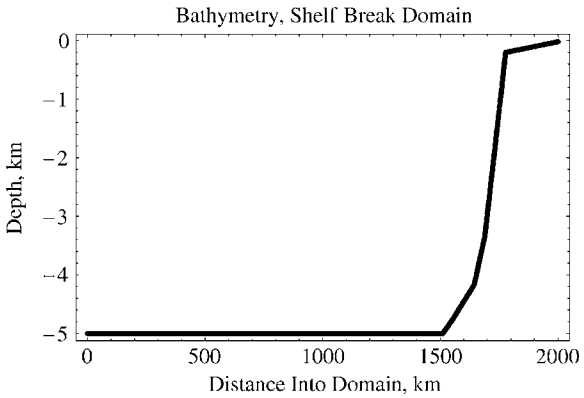


**Fig. 1.** Bathymetry for shelf break domain (adapted from Hagen et al. 2000)

a slice of an ocean shelf and basin (shown in Fig. 1); we will refer to it as the shelf break domain. It is an idealized version of the Western North Atlantic Ocean, as if a slice had been taken perpendicular to the United States coastline and extended into the deep ocean (Hagen et al. 2000). Local mass errors have been observed to occur in regions with rapidly changing bathymetry where the flow converges or diverges (Kolar et al. 1994). This domain contains a shelf break where the bathymetry increases rapidly from a depth of 200 m to a depth of 5 km, and thus it should be a good test of the model's local mass conservation and truncation error properties.

The first test on this domain has a constant grid spacing of about 44.4 km, which corresponds to 46 nodes. The second test on this domain has the same number of nodes, but they are variably spaced, as determined from the LTEA method (Hagen et al. 2000, 2001). The LTEA method places nodes based on the truncation errors associated with the discrete form of the linearized, harmonic conservation of momentum equation, and it has been shown to improve both accuracy and efficiency. The grid spacing ranges from about 112.5 km in the deep water to 1 km at the shelf break. Fig. 2 compares the two different node placements for the shelf break domain. Note that the LTEA method clusters nodes at a distance into the domain of about 1,750 km, which is where the break in the bathymetry occurs.

Both meshes share the following simulation parameters: a time step of 1 s, a simulation time of 3.24 M2 tidal cycles (or 40.24 h), a constant bottom friction of 0.0001 $s^{-1}$, a lateral eddy viscosity of zero, and a numerical $G$ parameter of 0.001 $s^{-1}$. They also

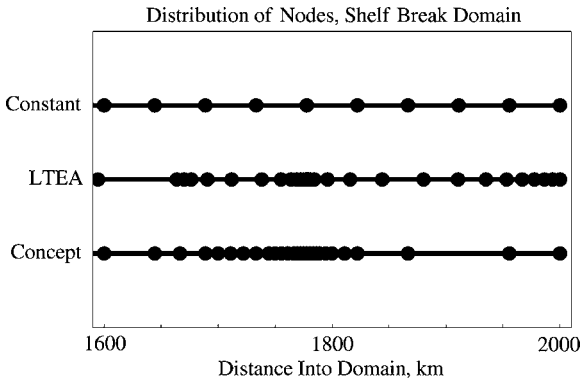


**Fig. 2.** Distribution of nodes for last 400 km of shelf break domain, for three meshes

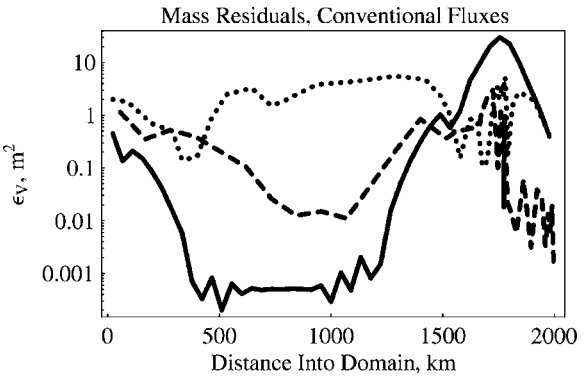


**Fig. 3.** Mass residuals $\varepsilon_V$ for one-dimensional domains. Shelf break (constant spacing) residuals are shown in solid line, shelf break (LTEA) residuals are shown in dashed line, and shelf break (concept) residuals are shown in dotted line.

share the same fine grid ("true") solution, which utilizes 8,193 nodes and a constant grid spacing of 244 m. This fine grid was obtained by refining the shelf break (constant spacing) domain until the solution converged to the sixth decimal place. We will present errors from the third to last time step in these simulations, so the elevation and velocity output from the fine grid solution was saved for the last five time steps and used to estimate the derivatives in the truncation error terms.

### *Shelf Break Domain—Constant Spacing*

The constant spacing version of the shelf break domain is an interesting test of both mass residuals and local truncation errors, because no attempt has been made to place nodes in a manner that minimizes error. The mass residuals $\varepsilon_V$ (which uses the conventional flux) and $\varepsilon_S$ (which uses the consistent fluxes) are shown as the solid lines in Figs. 3 and 4, respectively. The mass residual $\varepsilon_V$ is relatively small throughout most of the domain, except for the shelf break region, where the residual reaches a maximum magnitude of 29.9 $m^2$. (The normalized residuals, which we mention only as a means of comparison, would be in the range of $10^{-6}$–$10^{-3}$% of the deviation from the still water volume throughout most of the domain, and 0.6% of the deviation from the still water volume in the shelf break region.) In contrast, the mass residual $\varepsilon_S$ shows a steady increase throughout the domain, and its maximum magnitude of $1.6 \cdot 10^{-6}$ $m^2$ occurs at the land bound-

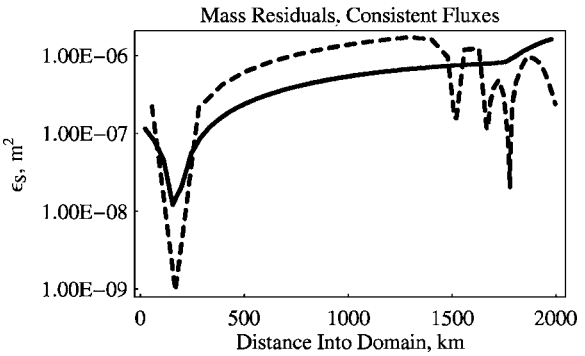


**Fig. 4.** Mass residuals $\varepsilon_S$ for one-dimensional domains. Shelf break (constant spacing) residuals are shown in solid line, and shelf break (LTEA) residuals are shown in dashed line.

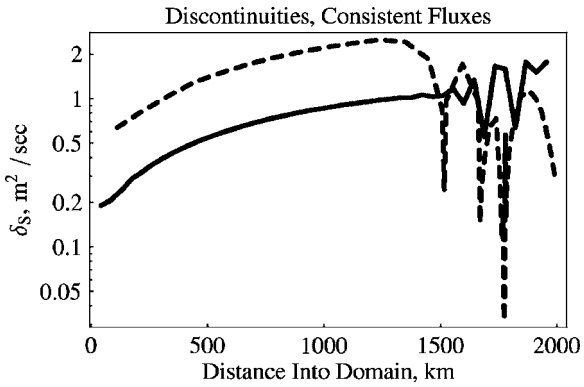


**Fig. 5.** Consistent flux discontinuities $\delta_S$ for one-dimensional domains. Shelf break (constant spacing) discontinuities are shown in solid line, and shelf break (LTEA) residuals are shown in dashed line.

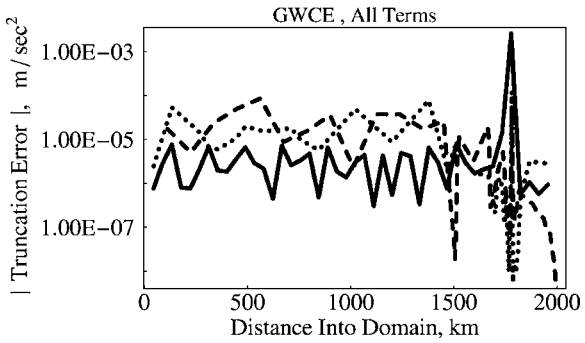


**Fig. 6.** Absolute values of truncation errors for all of terms in GWC equation, for one-dimensional domains. Shelf break (constant spacing) errors are shown in solid line, the shelf break (LTEA) errors are shown in dashed line, and shelf break (concept) errors are shown in dotted line.

ary on the right side of the domain. The third error norm, the consistent flux discontinuity $\delta_S$, is shown as a solid line in Fig. 5. The discontinuities increase throughout the domain, but there is a noticeable change in their behavior at the shelf break, where the discontinuities oscillate with a wavelength of $2\Delta x$.

We offer two observations based on the error norms themselves. First, the mass residuals based on the conventional fluxes are significantly larger than the mass residuals based on the consistent fluxes. This behavior is to be expected, because the consistent fluxes are derived in a manner that is consistent with the discretization of the governing equations, and they are evaluated using computed solutions for that element. However, because of the problems described above regarding the derivation of the consistent fluxes for the GWC equation, the mass residual $\varepsilon_S$ based on these fluxes does not perfectly conserve mass on the element level. Although the errors shown as the dashed line in Fig. 4 are small, they are too large to be round-off error. Second, only the mass residual $\varepsilon_V$ has its maximum at the shelf break, which is located at a distance of about 1,780 km into the domain. In contrast, the mass residual based on the consistent fluxes shows an obvious change in behavior at the shelf break, but its magnitude continues to increase on the shelf. The flux discontinuities $\delta_S$ also continue to increase on the shelf, and they show a $2\Delta x$ oscillation that is not seen in either of the other mass residual plots.

A summary of the truncation errors is shown in Table 1, and the spatial distribution of the truncation errors for all terms in the GWC and NCM equations are shown as solid lines in Figs. 6 and 7, respectively. The maximum truncation error for the GWC equation is $4.27 \cdot 10^{-3}$ m/s$^2$, and the maximum truncation error for the NCM equation is $2.07 \cdot 10^{-3}$ m/s$^2$. Table 1 also shows the correlations between the truncation errors associated with the terms in the governing equations and the mass and flux errors associated with the three norms $\varepsilon_V$, $\varepsilon_S$, and $\delta_S$. To perform this correlation, we computed Pearson's product-moment correlation coefficient, $r$, using the local truncation errors and each of the mass error norms; the correlation coefficients are shown in the last three columns of Table 1. Pearson's product-moment correlation coefficient is given by

$$r_{12} = \frac{\sum (Y_{i1} - \overline{Y_1})(Y_{i2} - \overline{Y_2})}{\sqrt{\sum (Y_{i1} - \overline{Y_1})^2 \sum (Y_{i2} - \overline{Y_2})^2}} \tag{21}$$

where $Y_1$ and $Y_2$=data sets and the overbar indicates a mean (Neter et al. 1996). The local truncation errors and the consistent flux discontinuities $\delta_S$ are node-based errors, whereas the mass residuals $\varepsilon_V$ and $\varepsilon_S$ are element based; to compute the correlation coefficient, we projected the mass residuals to the nodes by selecting the larger of the residuals from the two adjoining elements. This correlation coefficient can range between −1 and 1; for the purposes of mesh refinement, a coefficient of −1 might be just as useful as a coefficient of 1, because it would still represent a strong (albeit negative) correlation between truncation errors and mass errors. As shown in Table 1, the magnitudes of the correlation coefficients for the shelf break (constant spacing) domain are about 0.5 or less. However, it should be noted that the coefficients for $\varepsilon_V$ are about 2–3 times larger than the coefficients for $\varepsilon_S$ and $\delta_S$, indicating that the conventional fluxes produce mass residuals that are a much more useful predictor of truncation error in the model.

The final study in this section is convergence. As noted above, the local truncation errors for the GWC and NCM equations are formally second-order accurate in space, for constant-spacing domains. Recent studies, such as Dawson et al. (2006), indicate that second-order convergence rates can be observed in both the elevation and velocity solutions of GWCE-based models, under certain conditions involving the treatment of the boundary terms, the discretizations of the terms in the governing equations, and the design of the mesh. A similar convergence study for the shelf break (constant spacing) grid was conducted, in which the grid

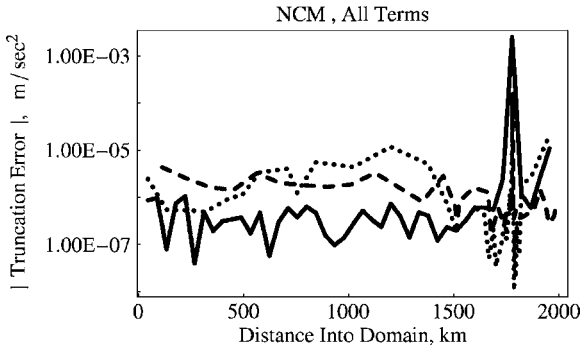


**Fig. 7.** Absolute values of truncation errors for all of terms in NCM equation, for one-dimensional domains. Shelf break (constant spacing) errors are shown in solid line, shelf break (LTEA) errors are shown in dashed line, and shelf break (concept) errors are shown in dotted line.

**Table 1.** Summary of Truncation Errors for Shelf Break (Constant Spacing) Domain

| Truncation error terms | | Max error ($m/s^2$) | Correlation coefficient $r$ | | |
|---|---|---|---|---|---|
| Nomenclature | Expression | | … to $\varepsilon_V$ | … to $\varepsilon_S$ | … to $\delta_S$ |
| **Generalized wave continuity equation** | | **2.56E-03** | **0.542** | **0.166** | **0.287** |
| First | $\partial^2\zeta/\partial t^2$ | 1.77E-05 | 0.556 | 0.063 | 0.281 |
| Second | $G(\partial\zeta/\partial t)$ | 1.33E-08 | 0.231 | 0.136 | 0.170 |
| Finite amplitude, Part 1 | $gh(\partial^2\zeta/\partial x^2)$ | 1.67E-03 | 0.541 | 0.167 | 0.287 |
| Finite amplitude, Part 2 | $g(\partial(\zeta^2)/\partial x^2)$ | 3.37E-06 | 0.541 | 0.167 | 0.287 |
| Advective, Part 1 | $\partial(U\partial\zeta/\partial t)/\partial x$ | 8.98E-07 | 0.540 | 0.167 | 0.286 |
| Advective, Part 2 | $\partial(HU\partial U/\partial t)/\partial x$ | 8.57E-04 | 0.541 | 0.167 | 0.287 |
| Flux | $(G-\tau)(\partial HU/\partial x)$ | 1.29E-05 | 0.554 | 0.171 | 0.293 |
| **Nonconservative momentum equation** | | **2.54E-03** | **0.541** | **0.170** | **0.289** |
| Accumulation | $\partial U/\partial t$ | 6.69E-05 | 0.539 | 0.179 | 0.293 |
| Advective | $U(\partial U/\partial x)$ | 5.51E-04 | 0.541 | 0.168 | 0.287 |
| Bottom friction | $\tau U$ | 3.76E-04 | 0.542 | 0.172 | 0.291 |
| Finite amplitude | $g(\partial\zeta/\partial x)$ | 1.55E-03 | 0.541 | 0.169 | 0.288 |

spacing was decreased systematically from 44.4 km to the minimum of 244 m used in our fine ("true") solution. This corresponds to an increase in the number of nodes from 46 to 8,193. Each grid spacing corresponds to a unique mesh; the root-mean-square (RMS) errors for elevation and velocity (which are global error metrics) were computed for each mesh by comparing the coarse solution to the "true" solution at the third-to-last time step. The convergence rates for elevation and velocity (not shown graphically herein) were found to be 1.75 and 1.13, respectively. The degradation of the convergence rates from the theoretical second-order rate, especially with respect to velocity, can be attributed to several factors, including the implementation of the boundary conditions and the nonlinear behavior in the shelf break region. For the velocity solution, the convergence rates at specific nodes in the domain (not shown graphically herein) are consistently second order, except in the shelf break region, where the convergence rates deteriorate to first order. This degradation of solution accuracy in the shelf break region limits the convergence rate of the global RMS error.

If the mass residuals are to be used as a surrogate for local truncation errors, then they should show similar convergence rates. For the same convergence study described above, the three error norms were computed for each mesh, and then a RMS norm was computed for each error. These RMS norms were then plotted over the range of grid spacings. The convergence behaviors for the mass residuals $\varepsilon_V$ and $\varepsilon_S$ are shown in Figs. 8 and 9, and the convergence behavior for the consistent flux discontinuities $\delta_S$ is shown in Fig. 10. Linear regressions through the points in these figures produce a slope of 1.44 for the mass residual $\varepsilon_V$ in Fig. 8 and slopes of unity for the error measures in Figs. 9 and 10. Thus, they converge at rates similar to those of the elevation (1.75) and velocity (1.13) solutions. In fact, this behavior is to be expected, because the error norms are functions of the solution, and thus their convergence rates should be similar to the convergence rate of the solution.

It should be noted that, if an $L_\infty$ norm is used instead of RMS, then all three mass residuals produce convergence rates near unity. While not representative of global behavior, the $L_\infty$ norm is a better metric for local error because it is a measure of the largest error in the domain; hence, we believe it is more useful in a grid refinement study that aims to minimize the largest errors. For that reason, we use the $L_\infty$ norm in our mesh refinement examples below.

### *Shelf Break Domain—LTEA*

As noted earlier, the shelf break (LTEA) domain was designed specifically to minimize local truncation error, and thus it should be expected that ancillary quantities are minimized as well. The mass residuals $\varepsilon_V$ and $\varepsilon_S$ for this domain are shown as dashed lines in Figs. 3 and 4, respectively. The residual $\varepsilon_V$, which is based on conventional fluxes, still has a peak in the shelf break region, but its maximum of 3.083 $m^2$ is an order of magnitude

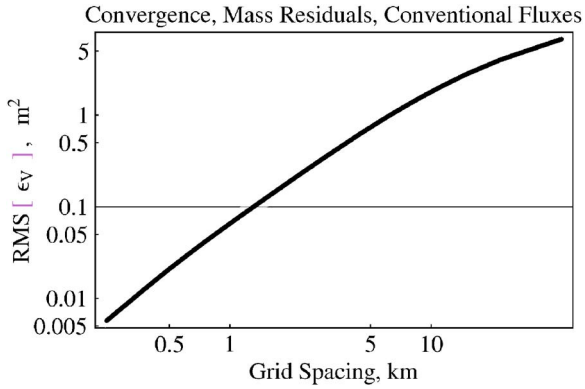


**Fig. 8.** Convergence behavior for mass residuals $\varepsilon_V$

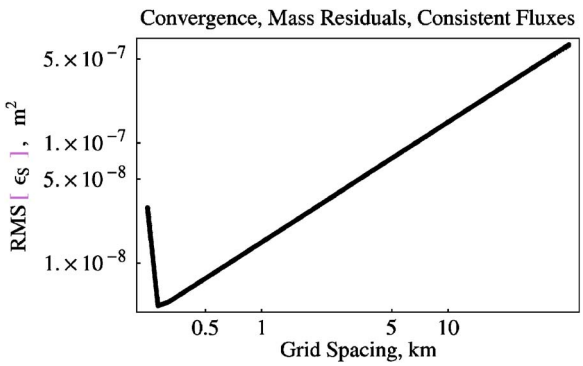


**Fig. 9.** Convergence behavior for mass residuals $\varepsilon_S$

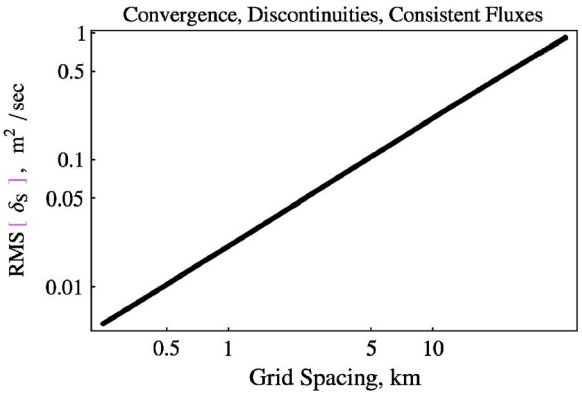


**Fig. 10.** Convergence behavior for mass residuals $\delta_S$

less than the maximum error in the shelf break (constant spacing) domain (shown as the solid line in Fig. 3) and on the same order of magnitude as the other errors in the domain. The residual $\varepsilon_S$, which is based on the consistent fluxes, now shows uniform errors throughout the domain. Its qualitative behavior again matches closely that of the consistent flux discontinuity $\delta_S$, which is shown as a dashed line in Fig. 5.

The truncation errors for the shelf break (LTEA) domain are summarized in Table 2, and the errors for the GWC and NCM equations are shown as dashed lines in Figs. 6 and 7, respectively. The LTEA method has its intended effect on the truncation errors; the maximum error for the GWC equation decreased by about two orders of magnitude, and the maximum error for the NCM equation decreased by more than one order of magnitude. In both cases, the peak at the shelf break still exists, but it is both smaller and narrower. A decrease in the error norm based on the conventional fluxes corresponds to a similar or larger decrease in the truncation errors. A qualitative comparison of the mass and truncation errors would suggest that the mass residual $\varepsilon_V$ (the dashed line in Fig. 3) correlates to the NCM truncation errors (the dashed line in Fig. 7), because both show a significant peak at the shelf break, and that the mass residual $\varepsilon_S$ (the dashed line in Fig. 4) correlates to the GWC truncation errors (the dashed line in Fig. 6), because both show uniform errors throughout the domain. The quantitative comparison in Table 2 lends support to this observation, although the correlations are relatively weak, and there is variability in the correlations on a term-by-term basis in both equations. More importantly, the LTEA method has succeeded in minimizing the maximum errors and distributing mass and truncation errors over the domain, and thus the correlation is not nearly as significant or uniform as it was in the shelf break (constant spacing) domain.

### *Summary*

The results of our analyses in one dimension indicate that the conventional fluxes produce mass residuals, $\varepsilon_V$, that are more strongly correlated with truncation errors. From the analysis with the shelf break (constant spacing) domain, we saw that: (1) the mass residuals were larger in magnitude, which supports the expectations produced during the derivation; (2) these residuals have their maximum at the shelf break itself, which is also where the truncation errors peak; and (3) this relationship can be quantified, as the correlation coefficients between the mass residuals and the truncation errors are two to three times larger than correlations using other error measures.

## Examples of Mesh Refinement Using Mass Residuals

It remains to be seen whether these mass residuals can be used as a practical error metric for mesh refinement. In this section, we present two examples of mesh refinement using the mass residuals, $\varepsilon_V$, based on the conventional fluxes. In the first example, we begin with the shelf break (constant spacing) domain and move nodes until the maximum mass residual is less than the corresponding maximum mass residual from the shelf break (LTEA) domain. In the second example, we begin with an irregular, two-dimensional mesh of the Bight of Abaco domain and add nodes until the maximum mass residual is less than a prescribed value.

### *Mesh Refinement in One Dimension*

In this section, we demonstrate the development of a grid that uses mass residuals as the criterion for mesh refinement. We begin with the shelf break (constant spacing) domain described above, and we make the following assumptions:

**Table 2.** Summary of Truncation Errors for Shelf Break (LTEA) Domain

| Truncation error terms | | Max error | Correlation coefficient $r$ | | |
|---|---|---|---|---|---|
| Nomenclature | Expression | ($m/s^2$) | … to $\varepsilon_V$ | … to $\varepsilon_S$ | … to $\delta_S$ |
| **Generalized wave continuity equation** | | **8.58E-05** | **−0.080** | **0.285** | **0.449** |
| First | $\partial^2\zeta/\partial t^2$ | 6.10E-05 | −0.139 | 0.442 | 0.581 |
| Second | $G(\partial\zeta/\partial t)$ | 3.87E-08 | −0.245 | 0.584 | 0.719 |
| Finite amplitude, Part 1 | $gh(\partial^2\zeta/\partial x^2)$ | 3.43E-05 | −0.030 | 0.118 | 0.263 |
| Finite amplitude, Part 2 | $g(\partial(\zeta^2)/\partial x^2)$ | 8.08E-08 | 0.085 | −0.222 | −0.133 |
| Advective, Part 1 | $\partial(U\partial\zeta/\partial t)/\partial x$ | 1.20E-07 | 0.072 | −0.170 | −0.026 |
| Advective, Part 2 | $\partial(HU\partial U/\partial t)/\partial x$ | 1.69E-05 | 0.101 | −0.266 | −0.180 |
| Flux | $(G-\tau)(\partial HU/\partial x)$ | 4.75E-06 | 0.152 | −0.231 | −0.219 |
| **Nonconservative momentum equation** | | **1.67E-04** | **0.074** | **−0.176** | **−0.057** |
| Accumulation | $\partial U/\partial t$ | 2.95E-06 | −0.166 | 0.473 | 0.592 |
| Advective | $U(\partial U/\partial x)$ | 7.27E-05 | 0.078 | −0.189 | −0.077 |
| Bottom friction | $\tau U$ | 2.15E-06 | 0.135 | −0.316 | −0.224 |
| Finite amplitude | $g(\partial\zeta/\partial x)$ | 9.16E-05 | 0.079 | −0.191 | −0.074 |

**Table 3.** Summary of Truncation Errors for Shelf Break (Concept) Domain

| Truncation error terms | | Max error ($m/s^2$) | Correlation coefficient $r$ | | |
|---|---|---|---|---|---|
| Nomenclature | Expression | | … to $\varepsilon_V$ | … to $\varepsilon_S$ | … to $\delta_S$ |
| **Generalized wave continuity equation** | | **1.24E-04** | **0.403** | **0.166** | **–0.203** |
| First | $\partial^2\zeta/\partial t^2$ | 5.27E-05 | 0.248 | 0.085 | –0.441 |
| Second | $G(\partial\zeta/\partial t)$ | 6.25E-08 | 0.316 | –0.043 | –0.722 |
| Finite amplitude, Part 1 | $gh(\partial^2\zeta/\partial x^2)$ | 8.15E-05 | 0.377 | 0.159 | –0.050 |
| Finite amplitude, Part 2 | $g(\partial(\zeta^2)/\partial x^2)$ | 1.93E-07 | 0.299 | 0.141 | 0.097 |
| Advective, Part 1 | $\partial(U\partial\zeta/\partial t)/\partial x$ | 1.65E-08 | 0.325 | –0.012 | –0.515 |
| Advective, Part 2 | $\partial(HU\partial U/\partial t)/\partial x$ | 4.12E-05 | 0.295 | 0.141 | 0.108 |
| Flux | $(G-\tau)(\partial HU/\partial x)$ | 1.13E-06 | 0.317 | 0.142 | 0.077 |
| **Nonconservative momentum equation** | | **2.11E-05** | **0.449** | **0.138** | **–0.649** |
| Accumulation | $\partial U/\partial t$ | 1.08E-05 | 0.433 | 0.090 | –0.679 |
| Advective | $U(\partial U/\partial x)$ | 2.52E-06 | 0.400 | 0.186 | –0.166 |
| Bottom friction | $\tau U$ | 4.73E-06 | 0.175 | 0.067 | –0.441 |
| Finite amplitude | $g(\partial\zeta/\partial x)$ | 9.47E-06 | 0.351 | 0.134 | –0.486 |

1. The criterion should be the mass residual $\varepsilon_V$, which is based on the conventional fluxes, because we have shown that this residual is a better indicator of truncation errors than the error norms $\varepsilon_S$ and $\delta_S$, which are based on the consistent fluxes;
2. The total number of nodes should remain constant. In other words, in order to place a node in a region with large mass residuals, a node must first be removed from a region with small mass residuals. The shelf break (constant spacing) domain has 46 nodes;
3. The removal of a node in a region with low mass balance errors should not affect the neighboring nodes. Thus, when a node is removed, its neighbors should not be moved to compensate. In effect, the grid spacing in that region is doubled, and it can be increased further during successive iterations;
4. When a node is added to a region with high mass balance errors, it should be placed at the midpoint of an existing element. In effect, the grid spacing in that region is halved; and
5. When a node is added, its bathymetry should be computed from a linear interpolation of the surrounding bathymetries. In an automated mesh-refinement scheme, a background grid and higher order interpolation could be used to compute bathymetries. However, this is not a concern in this example, because the shelf break (constant) domain uses linear segments of bathymetry, as shown in Fig. 1.

These assumptions were made as much for convenience as for scientific correctness. (It should be noted that some of these assumptions, such as the effective "doubling" of grid spacing when a node is removed, do not have convenient analogues in two dimensions.) Nonetheless, they allow for a grid development scenario that illustrates how mass residuals can be used to generate a mesh that minimizes truncation errors. And, by keeping the number of nodes constant, we can compare our concept mesh to the LTEA mesh with 46 nodes. Future work would automate this procedure; for now, the mesh is refined iteratively, by moving five nodes at a time and then generating an updated solution.

We begin with the mass residuals $\varepsilon_V$ based on the conventional fluxes shown in Fig. 3. For the shelf break (constant spacing) domain, the largest magnitude error is about 29.9 $m^2$, and it occurs at a distance of about 1,780 km, which is near where the continental shelf begins its steep descent, as shown in Fig. 1. All of the significant mass residuals occur in this region. Thus, to minimize these mass residuals, we remove nodes from the deeper parts of the domain and add them to the shelf-break region. After four iterations, in which we move five nodes at a time and recompute the mass residuals, we obtain the node placement depicted at the bottom of Fig. 2.

We can make several observations based solely on the node distribution. First, in order to minimize the mass residuals $\varepsilon_V$, the majority of the nodes were placed in the region where the shelf begins its steep descent (at a distance of about 1,800 km). The grid spacing in this region is about 2,700 m, or 16 times smaller than the original constant node spacing. Second, to effect this decrease in the node spacing along the shelf break, we removed nodes from the deep water portion of the domain. The grid spacing in the deep water portion was increased to as high as 177,000 m, or four times larger than the original grid spacing. Third, after four iterations, a total of 20 nodes were moved during the mesh development.

The effect of this mesh on simulation results is dramatic. The mass residuals $\varepsilon_V$ are shown as a dotted line in Fig. 3. Adding nodes at the shelf break decreases the mass residuals in that region, and removing nodes from the deep water increases the mass residuals in that region (compared to the results from the regular mesh shown as the solid line in Fig. 3). The end result is a domain that has a more uniform distribution of error. Note that the largest magnitude residual is 5.53 $m^2$, which is a decrease of about 81% from the maximum residual produced by the original, constant-spacing mesh. Further iteration on node placement, using a more sophisticated method that placed nodes at locations other than the midpoint of elements and that limited the relative change of adjacent elements, would further decrease these mass residuals.

Similar behavior is observed with respect to truncation errors. The dotted line in Fig. 6 shows the truncation errors for all of the terms in the GWC equation, and the dotted line in Fig. 7 shows the truncation errors for all of the terms in the NCM equation. Note that, although both figures depict peaks at the shelf break, there are nontrivial truncation errors in the deep water region of the domain. Qualitatively, the truncation errors match well the mass residuals $\varepsilon_V$; i.e., they are distributed throughout the domain.

It is important to examine the effect of this mesh refinement in comparison to the original shelf break (constant spacing) domain

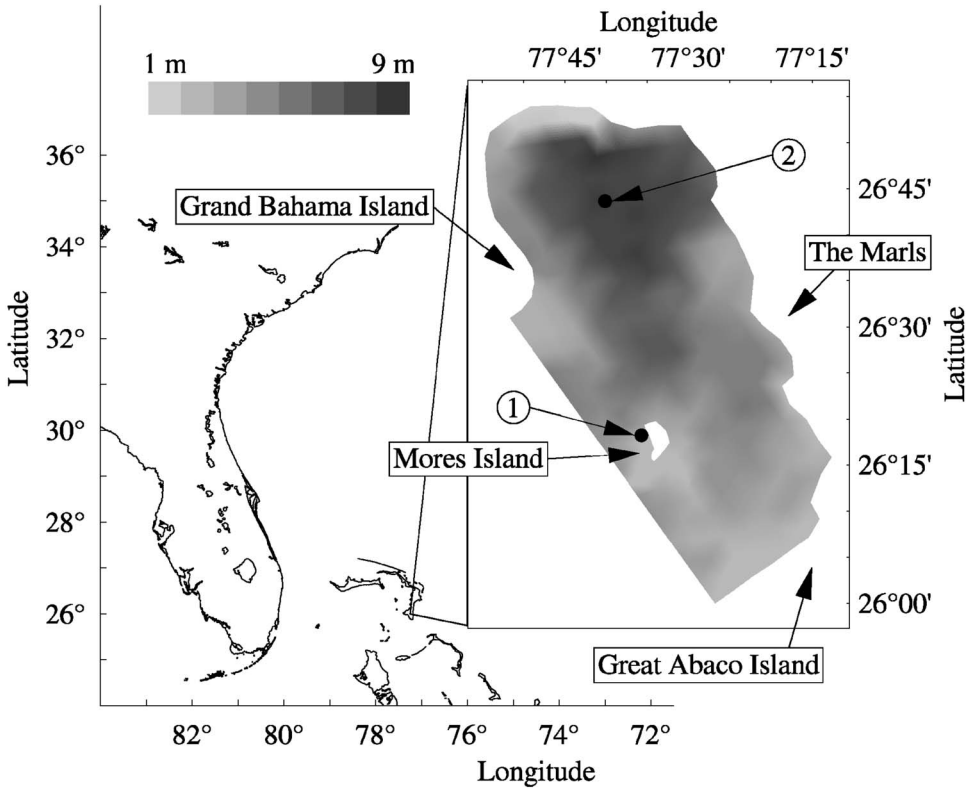


**Fig. 11.** Bathymetry of Bight of Abaco, Bahamas, domain with tidal recording stations indicated in figure (adapted from Grenier et al. 1995)

and to the shelf break (LTEA) domain, which was developed by minimizing local truncation error of the linearized, harmonic momentum equation. Table 3 summarizes the truncation errors for the shelf break (concept) domain. Note that the truncation errors from the concept domain are considerably smaller than those for the constant-spacing domain. An 81% decrease in the maximum mass residual $\varepsilon_V$ created a decrease of one order of magnitude in the maximum truncation error for the GWC equation and a decrease of two orders of magnitude in the maximum truncation error for the NCM equation. Also note that the truncation errors from the concept domain are comparable to those from the LTEA domain; in fact, the NCM truncation errors are smaller in the concept domain. [This behavior is most likely due to the fact that Hagen et al. (2000, 2001) used the linear harmonic form of the NCM equation to develop the shelf break (LTEA) domain, whereas this study uses the full, nonlinear, transient form of the

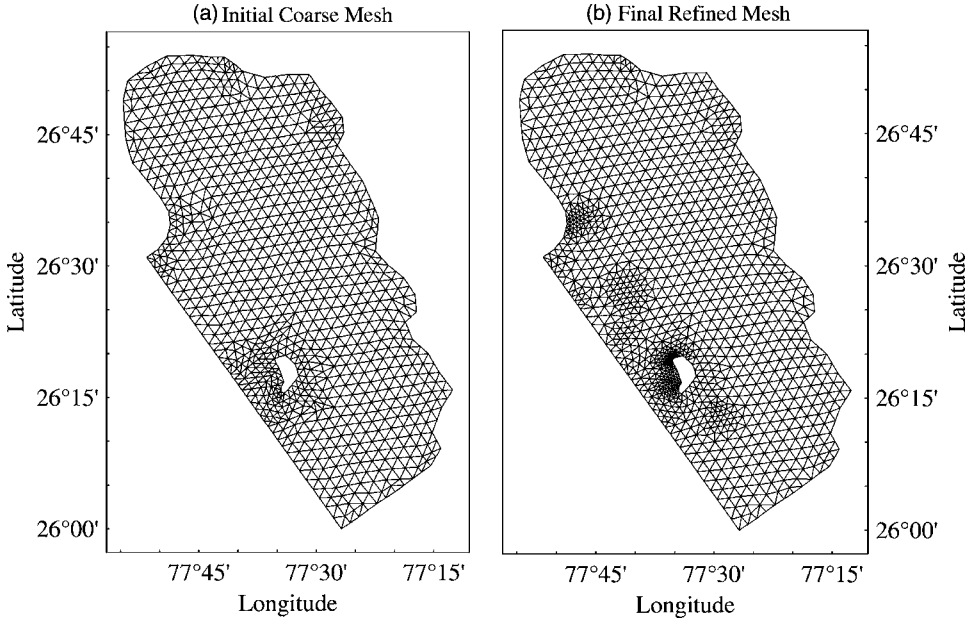


**Fig. 12.** Meshes of refinement study: (a) initial coarse mesh of 926 nodes; (b) final refined mesh of 1,178 nodes

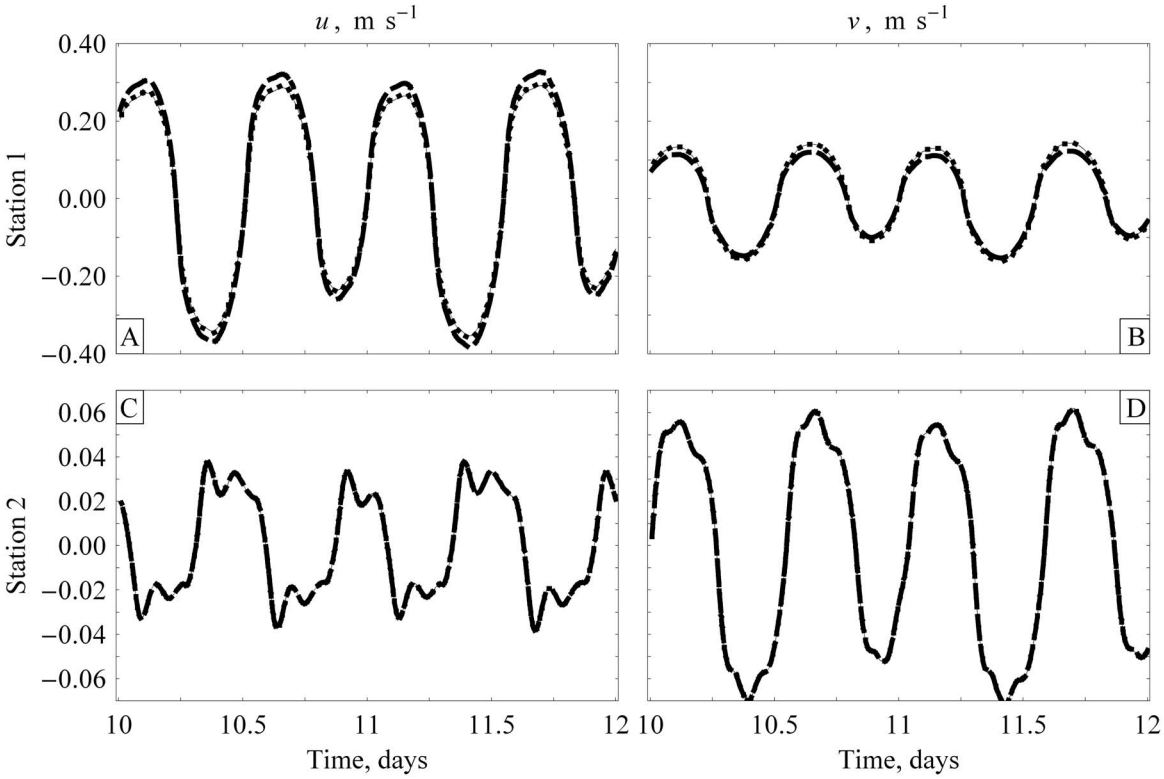


**Fig. 13.** Velocity station graphs for Stations 1 and 2, whose locations are shown in Fig. 11. (A) and (C) show $x$ component of velocity, and (B) and (D) show $y$ component of velocity. Dashed line shows results from initial mesh, dotted line shows results from refined mesh, and solid line shows results from "true" solution.

NCM equation.] Thus, not only does this method of mesh refinement decrease the truncation errors, it does so as effectively as a grid that was developed by explicitly minimizing truncation errors.

It should be noted that the correlation coefficients for $\varepsilon_V$ and the shelf break (concept) domain in Table 3 are significantly better than the respective correlation coefficients for the shelf break (LTEA) domain in Table 2. Even after we moved 20 nodes and produced a nonuniform mesh that minimizes both mass residuals and truncation error, the correlations are still 0.403 for the GWC equation and 0.449 for the NCM equation. The respective correlations for the shelf break (LTEA) domain are −0.080 and 0.074. Thus, even at this stage in the mesh refinement process, the mass residual $\varepsilon_V$ can still be used as a criterion for further refinement; its utility is not lost.

In summary, by beginning with a mesh that had a constant node spacing and then moving nodes to minimize the mass residual $\varepsilon_V$ based on the conventional fluxes, we developed a mesh that decreased the maximum mass residual by 81% and decreased the maximum truncation errors by one or two orders of magnitude. In effect, we replicated the positive qualities of the shelf break (LTEA) domain without having to compute any truncation errors during the refinement of the mesh.

### *Mesh Refinement in Two Dimensions*

In this section, we test the concept of using elemental mass residuals as a criterion for mesh refinement in a two-dimensional setting. In particular, we examine the Bight of Abaco, Bahamas domain; Fig. 11 shows the bathymetry of the area. Land boundaries, consisting of the islands around the bight, are treated as no flow boundaries, while the ocean boundary between the islands of Abaco and Grand Bahama along the southwest edge of the domain is forced with five tidal constituents: $O1$, $K1$, $N2$, $M2$, and $S2$. The coarse mesh for this domain consists of 1,696 nonuniform elements and 926 nodes, as shown in Fig. 12(A). Other parameters for the simulation are as follows: bottom friction factor in the Chezy formulation of 0.009, lateral eddy viscosity of zero, numerical $G$ parameter of 0.009 $s^{-1}$, time step of 10 s, Coriolis parameter of $5.9 \cdot 10^{-5}$ $s^{-1}$, and a simulation time of 12 days. After a 10-day spinup, simulation results were recorded over the last 2 days, and elevation and velocity changes were analyzed at stations throughout the domain. A true solution was established by successively refining the mesh until the time series data no longer showed significant differences from the previous iteration; each iteration quadrupled the number of elements. It was found that the solution converged after the second refinement, thus a grid consisting of 27,136 elements and 13,880 nodes was used as the true solution.

The mesh refinement procedure was similar to that used in the one-dimensional example above, in that the criterion for refinement was the mass residual $\varepsilon_V$. However, a LTEA grid for this domain does not exist, so we could not use its mass balance and truncation error properties as the goal of our concept domain. Thus, instead of moving around the existing nodes as we did in the one-dimensional example, we simply added nodes in regions with large mass residuals. After each iteration, these regions were refined until the absolute residuals were an order of magnitude less (chosen arbitrarily for this proof-of-concept application) than

those of the coarse grid. Other differences from the procedure used in the one-dimensional example are as follows: (1) elemental residuals were aggregated to node points because the mesh generation software is nodal based ("hand" refinements without the nodal aggregation showed similar results, although the aggregation process tended to space out errors among patches of elements instead of single elements); (2) after a particular region was refined, we "relaxed" the mesh in the adjacent area in order to provide a smooth transition from fine to coarse elements and to avoid poorly proportioned triangles; and (3) we did not remove nodes from portions of the mesh with lower mass residuals because the original resolution was the minimum needed to resolve all constituents and their nonlinear interactions (Grenier et al. 1995).

Results show that, with only one refinement iteration, nearly the entire domain met the criteria of lowering elemental mass residuals by an order of magnitude. In fact, the only area that exceeded the criterion was a small patch of elements near the Mores Island (see Fig. 11). Two more iterations of selective mesh refinements in this area succeeded in meeting the criterion over the entire domain. Fig. 12(A) shows the initial coarse mesh (1,696 elements and 926 nodes), while Fig. 12(B) shows the final refined mesh (2,180 elements and 1,178 nodes). Comparing these two figures, we note that the refinement occurred in areas with either a steep topography change or where the velocity field is forced to change direction because of the presence of a land boundary, e.g., note the areas of refinement in Fig. 12(B) around Mores Island and near the Grand Bahamas Island. This behavior is consistent with past observations of the need to provide increased resolution in areas of rapidly changing topography or high advective gradients (Hagen et al. 2001).

After each refinement, we compared simulation results from the elevation and velocity stations to the true solution. For all of the stations, we found that there is no significant change in the elevation response between the different meshes; however, changes in the velocity field depend on location within the domain. To simplify the discussion, we present results from only two of the stations; the locations of these stations are shown in Fig. 11, and the velocity results at these stations are shown in Fig. 13. In Figs. 13(A) and 13(B), we show the velocity results for Station 1, which is near Mores Island and in a region that needed refinement. For the initial coarse mesh (dashed line), the velocity is either under- or overpredicted for each tidal cycle, as compared to the true solution (solid line). However, with three iterations of mesh refinement, the velocity results (dotted line) match the true solution. Remarkably, a mere 27% increase in the number of nodes produces a result that is as accurate as the mesh used for the true solution, which had a 1,400% increase in the number of nodes. In Figs. 13(C) and 13(D), we show the velocity results for Station 2, which is located in a region that did not need refinement. Note that the velocity field is unaffected by the mesh refinement; all three lines plot on top of each other. These results indicate that the mesh refinement influences results locally for this domain, although we temper this with observations from other studies that refinement can influence far-field regions (Hagen et al. 2000, 2001; Luettich and Westerink 1995). Finally, it is interesting to note that this type of station response follows that seen in previous studies, wherein the velocity solution is more significantly affected than elevations by variation in the numerical parameter $G$, which also significantly impacts local mass balance (Kolar et al. 1994).

## Conclusions

In this paper, we investigated local mass residuals as a criterion for mesh refinement. In a pair of examples using an idealized one-dimensional shelf break domain, we showed that mass residuals based on conventional fluxes correlate more strongly with truncation errors than did our other error norms based on consistent fluxes, and thus are a better indicator of problem areas. Then, in examples in one and two dimensions, we demonstrated the development of meshes by minimizing local mass residuals. In one dimension, the resulting mesh exhibited: (1) mass residuals that were better than the constant-spacing domain and slightly larger than the LTEA mesh; and (2) truncation errors that were comparable to or better than the truncation errors produced by the LTEA mesh. In two dimensions, the maximum mass residual was decreased by an order of magnitude after only three iterations of refinement, and the velocity stations in the regions of refinement agreed with the true solution. Consequently, mass residuals based on a conventional flux calculation show real promise as a criterion for mesh refinement, particularly because they can be incorporated into a dynamic meshing algorithm.

## Acknowledgments

The writers would like to thank Evan Tromble and Ian Toohey of the University of Oklahoma for their help in the completion of the mesh refinement example in two dimensions. The authors would also like to thank Dr. Joannes Westerink of the University of Notre Dame for his help in the completion of the convergence study in one dimension. The authors acknowledge funding from the National Defense Science and Engineering Graduate Fellowship from the Department of Defense, the Office of Naval Research under Grant No. N00014-02-1-0651, and the Department of Education through the GAANN Program. Any opinions, findings, conclusions, and recommendations expressed in this material are those of the authors and do not necessarily reflect those of the funding agencies.

## References

Atkinson, J. H., Westerink, J. J., and Hervouet, J. M. (2004). "Similarities between the quasi-bubble and the generalized wave continuity equation solutions to the shallow water equations." *Int. J. Numer. Methods Fluids*, 45, 689–714.

Baker, T. J. (1997). "Mesh adaptation strategies for problems in fluid dynamics." *Finite Elem. Anal. Design*, 25, 243–273.

Behrens, J. (1998). "Atmospheric and ocean modeling with an adaptive finite-element solver for the shallow-water equations." *Appl. Numer. Math.*, 26, 217–226.

Berger, M. J., and Jameson, A. (1985). "Automatic adaptive grid refinement for the Euler equations." *AIAA J.*, 23, 561–568.

Berger, M. J., and Oliger, J. (1984). "Adaptive mesh refinement for hyperbolic partial differential equations." *J. Comput. Phys.*, 53, 484–512.

Berger, R. C., and Howington, S. E. (2002). "Discrete fluxes and mass balance in finite elements." *J. Hydraul. Eng.*, 128(1), 87–92.

Cascon, J. M., Garcia, G. C., and Rodriguez, R. (2003). "A priori and a posteriori error analysis for a large-scale ocean circulation finite-element model." *Comput. Methods Appl. Mech. Eng.*, 192, 5305–5327.

Dawson, C., Westerink, J. J., Feyen, J. C., and Pothina, D. (2006). "Continuous, discontinuous, and coupled discontinuous-continuous

Galerkin finite-element methods for the shallow water equations." *Int. J. Numer. Methods Fluids*, in press.
Dresback, K. M. (2005). "Algorithmic improvements and analyses of the generalized wave continuity equation based model, ADCIRC." Ph.D. dissertation, Univ. of Oklahoma, Norman, Okla., 208–214.
Grenier, R. R., Luettich, R. A., and Westerink, J. J. (1995). "A comparison of the nonlinear frictional characteristics of two-dimensional and three-dimensional models of a shallow tidal embayment." *J. Geophys. Res.*, 100, 13719–13735.
Gresho, P. M., and Lee, R. L. (1981). "Don't suppress the wiggles—They're telling you something." *Comput. Fluids*, 9, 223–253.
Hagen, S. C., Westerink, J. J., and Kolar, R. L. (2000). "One-dimensional finite-element grids based on a localized truncation error analysis." *Int. J. Numer. Methods Fluids*, 32, 241–261.
Hagen, S. C., Westerink, J. J., Kolar, R. L., and Horstmann, O. (2001). "Two-dimensional, unstructured mesh generation for tidal models." *Int. J. Numer. Methods Fluids*, 35, 659–686.
Horritt, M. S. (2002). "Evaluating wetting and drying algorithms for finite-element models of shallow water flow." *Int. J. Numer. Methods Fluids*, 55, 835–851.
Hughes, T. J. R., Engel, G., Mazzei, L., and Larson, M. G. (2000). "The continuous Galerkin method is locally conservative." *J. Comput. Phys.*, 163(2), 467–488.
Kinnmark, I. P. E. (1984). "A two-dimensional analysis of the wave equation model for finite-element tidal computations." *Int. J. Numer. Methods Eng.*, 20, 369–383.
Kinnmark, I. P. E. (1985). "Stability and accuracy of spatial approximations for wave equation tidal models." *J. Comput. Phys.*, 60, 447–466.
Kinnmark, I. P. E. (1986). "The shallow water wave equations: Formulations, analysis and application." *Lecture notes in engineering*, C. A. Brebbia and S. A. Orsszag, eds., Vol. 15, Springer, Berlin, 187.
Kolar, R. L., Gray, W. G., and Westerink, J. J. (1996). "Boundary conditions in shallow water models: An alternative implementation for finite- element codes." *Int. J. Numer. Methods Fluids*, 22, 603–618.
Kolar, R. L., and Westerink, J. J. (2000). "A look back at 20 years of GWC-based shallow water models." *Proc., 13th Int. Conf. on Computational Methods in Water Resources*, Bentley, et al., eds., Balkema, Rotterdam, The Netherlands, 899–906.
Kolar, R. L., Westerink, J. J., Cantekin, M. E., and Blain, C. A. (1994). "Aspects of nonlinear simulations using shallow-water models based on the wave continuity equation." *Comput. Fluids*, 23, 523–538.
Lee, D., and Tsuei, Y. M. (1993). "A hybrid adaptive gridding procedure for recirculating fluid flow problems." *J. Comput. Phys.*, 108, 122–141.
Luettich, R. A., Hench, J. L., Fulcher, C. W., Werner, F. E., Blanton, B. O., and Churchill, J. H. (1999). "Barotropic tidal and wind driven larval transport in the vicinity of a barrier island inlet." *Int. J. Jap. Soc. Fish. Oceanogr.*, 8(2), 190–209.
Luettich, R. A., and Westerink, J. J. (1992). "ADCIRC: An advanced three-dimensional circulation model for shelves, coasts and estuaries. Report 1: Theory and methodology of ADCIRC-2DDI and ADCIRC-3DL." *Technical Rep. No. DRP-92-6*, Dept. of the Army, USACE, Washington, D.C.
Luettich, R. A., and Westerink, J. J. (1995). "Continental shelf scale convergence studies with a tidal model." *Quantitative skill assessment for coastal ocean models*, D. R. Lynch and A. M. Davies, eds., Vol. 47, American Geophysical Union, Washington, D.C., 349–371.
Lynch, D. R. (1985). "Mass balance in shallow water simulations." *Commun. Appl. Numer. Methods*, 1(4), 153–159.
Lynch, D. R., and Gray, W. G. (1979). "A wave equation model for finite-element tidal computations." *Comput. Fluids*, 7, 207–228.
Lynch, D. R., Ip, J. T. C., Naimie, F. E., and Werner, F. E. (1996). "Comprehensive coastal circulation model with application to the Gulf of Maine." *Cont. Shelf Res.*, 16, 875–906.
Marrocu, M., and Ambrosi, D. (1999). "Mesh adaptation strategies for shallow water flow." *Int. J. Numer. Methods Fluids*, 31, 497–512.
Massey, T. C., and Blain, C. A. (2006). "In search of a consistent and conservative mass flux for the GWCE." *Comput. Methods Appl. Mech. Eng.*, 195, 571–587.
Mewis, P., and Holtz, K. P. (1993). "A quasi bubble-function approach for shallow water waves." *Advances in Science and Engineering: Proc., 1st Int. Conf. on Hydro-Science and Engineering*, Vol. 1, Washington, D.C., Center for Computational Hydroscience and Engineering, School of Engineering, Univ. of Mississippi, 768–774.
Neter, J., Kutner, M. H., Nachtsheim, C. J., and Wasserman, W. (1996). *Applied linear statistical models*, McGraw-Hill, Chicago, 641.
Norton, W. R., King, I. P., and Orlob, G. T. (1973). "A finite-element model for lower granite reservoir." *Rep. Prepared by Water Resources Engineers, Inc., Walnut Creek, Calif., for Walla Walla District*, U.S. Army Corps of Engineers, Walla Walla, Wash.
Westerink, J. J., et al. (2008). "A basin to channel scale unstructured grid hurricane storm surge model for southern Louisiana." *Mon. Weather Rev.*, in press.
Wille, S. O. (1998). "Adaptive finite-element simulations of the surface currents in the North Sea." *Comput. Methods Appl. Mech. Eng.*, 166, 379–390.